S_2 + Air Combustion: Reaction Kinetics, Flame Structure, and Laminar Flame Behavior

N. Sebbar,*[,†] T. Zirwes,[‡] P. Habisreuther,[†] J. W. Bozzelli,[§] H. Bockhorn,[†] and D. Trimis[†]

[†]Combustion Technology, Engler Bunte Institute, Karlsruhe Institute of Technology (KIT), Engler Bunte Ring 7, 76131 Karlsruhe, Germany

[‡]Steinbuch Centre for Computing, Karlsruhe Institute of Technology (KIT), Hermann von Helmholtz Platz 1, 76344 Eggenstein Leopoldshafen, Germany

[§]Chemical Engineering Department, New Jersey Institute of Technology (NJIT), Newark, New Jersey 07102, United States

ABSTRACT: The paper presents a study on the combustion of S_2 over a wide range of air/fuel ratios, employing numerical flame calculations, including a sulfur/oxygen reaction mechanism; reaction zone structures as well as the corresponding laminar burning velocities are reported. The numerical simulations are based on a detailed reaction mechanism derived from a H/O/S combustion mechanism from the literature after removing all reactions of hydrogen containing species. Using reaction rate coefficients from the literature in the calculations brings about burning velocities in the order of magnitude of 300 cm s^{-1} at T_0 = 373 K and under stoichiometric conditions. Sensitivity analysis of the computed results identified which reaction rate has crucial influence on the burning velocity and flame structure. It turned out that the sensitivity coefficients of burning velocity with respect to the rate coefficient of reaction S + O_2 → SO + O are by far the largest sensitivity coefficients. Further investigations have been performed on the basis of different values of the rate constant of reaction S + O_2 → SO + O taken from the literature and from our own calculations. The obtained significant changes in burning velocities as well as in species profiles elucidate the sensitivity of the burning velocity and flame structure on the magnitude of the reaction rate coefficient of this reaction and stress the importance of this reaction. This work constitutes a necessary and to be continued footstep toward a validated reaction mechanism for the combustion of sulfur.

1. INTRODUCTION

This work is part of a collaborative European research project investigating a novel power cycle for renewable electricity production. The basic step of this power cycle is the thermal decomposition of sulfuric acid into SO_2, O_2, and H_2O at temperatures above 800 °C. The necessary energy is fed via a solar centrifugal particle receiver into the process. In a following process step, SO_2 disproportionates into S and sulfuric acid. Part of the received solar energy thereby is stored in sulfur, and combustion of sulfur releases again the stored energy, enabling the extension of electricity generation for baseload operation.[1] Within that cycle, combustion of sulfur should occur under hydrogen free conditions to avoid corrosion as a result of sulfuric acid formation. For the design of optimized combustion devices providing high power densities, the knowledge of combustion properties, such as laminar burning velocities, is necessary. Prerequisites for estimating burning velocities are validated reaction mecha nisms. Detailed reaction mechanisms involving only sulfur and oxygen species are therefore required. The present study is a first step in developing reaction mechanisms and to gain insight into the dynamics of heat release and flame structure of sulfur combustion.

Sulfur is a very cost effective material and can be inexpensively transported and stored outdoors under ambient conditions for long times and in large quantities.[2] Despite the fact that combustion of elemental sulfur is being performed for a long time on a large scale as part of the industrial production process of sulfuric acid and sulfuric acid being one of the world's largest volume industrial chemicals, little data concerning details of the combustion of sulfur are available in the literature. This is attributed, on the one hand, to the fact that experiments are difficult to perform because of the complicated rheological behavior of sulfur. On the other hand, the necessity to have a hydrogen free system to avoid corrosion as a result of sulfuric acid hampers any experimental investigation.

Several experimental and numerical studies for reaction of sulfur and sulfur containing compounds in different oxidizing atmospheres have been performed, and reaction mechanisms for the C/H/O/N/S system are reported in the literature. The scope of most reaction mechanisms from the literature is to describe the reactions of sulfur compounds in combination with hydrocarbon or hydrogen combustion (mostly motivated by the technically applied Claus process). However, none of them considers the oxidation of molecular sulfur in the absence of hydrogen or hydrocarbons, and therefore, the rate coefficients of reactions in the C/H/O/N/S system may be improper for use in pure sulfur/oxygen systems. One comprehensive reaction mechanism involving 67 reactions was reported by Glarborg et al. in 1996 and focused on the impact of SO_2 and NO on CO oxidation in the presence of

hydrogen.[3] Alzueta et al.[4] extend this mechanism to 82 reactions based on an experimental and theoretical study of the interaction of SO_2 with the radical pool present under combustion conditions. In a continuing study[5] the effect of the presence of SO_2 on CO oxidation in a CO_2 atmosphere as representative for oxy fuel combustion has been investigated and compared to combustion in a N_2 atmosphere, character istic for combustion with air. Glarborg and Marshall[6] recently developed a detailed chemical kinetic model (30 reactions) for oxidation of carbonyl sulfide (OCS) based on a critical evaluation of data from the literature. More recently, Song et al.[7] have conducted experiments on hydrogen sulfide oxidation in O_2/N_2 at a high pressure and developed a reaction mechanism with 44 reactions. Mueller et al.[8] have reported on kinetic modeling of the $CO/H_2O/O_2/NO/SO_2$ system and proposed a mechanism with 180 reactions. Zhang et al.[9] present a detailed kinetic mechanism for the homogeneous decomposition of SO_3–H_2O (sulfuric acid) vapor in the sulfur–iodine cycle. The kinetic mechanism involving 27 reactions and 11 species has been validated by experimental results.

As far as the above referenced literature comprises combustion or oxidation of sulfur, the developed reaction mechanisms contain the reaction $S + O_2 \rightarrow SO + O$.[3,4,6,7] It turns out by applying sensitivity analysis (presented and discussed in detail in section 2.2.1) that, for combustion of sulfur with air in a hydrogen and carbon free system, the sensitivity coefficient of burning velocity with respect to the rate coefficient of this reaction is by far the highest sensitivity coefficient. Therefore, the following discussion is focused to begin with on this reaction.

The reaction rate coefficients from the literature discussed below for the reaction $S + O_2 \rightarrow SO + O$ are given the three parameter form of k (cm^3 mol^{-1} s^{-1}) $= AT^b \exp(-T_A/T)$, in which T_A (K) $= E_a/R$. Woiki and Roth[10] have investigated the oxidation of S and SO by O_2 at high temperature conditions ($1220 \leq T \leq 3460$ K) with shock tube experiments and report a rate coefficient showing Arrhenius temperature dependency

$$S + O_2 \rightarrow SO + O \qquad 4.2 \times 10^{13} \quad 0.0 \quad 3110 \qquad (1)$$

giving then $k(1600\ \text{K}) = 6.01 \times 10^{12}$ cm^3 mol^{-1} s^{-1}.

Similar experiments from Tsuchiya et al.[11] reexamined that reaction and brought about

$$S + O_2 \rightarrow SO + O \qquad 1.52 \times 10^{13} \quad 0.0 \quad 1840 \qquad (2)$$

leading to $k(1600\ \text{K}) = 4.81 \times 10^{12}$ cm^3 mol^{-1} s^{-1} and also an Arrhenius type temperature dependency.

Lu et al.[12] investigated experimentally the reaction $S + O_2$ in argon at 50 Torr in the temperature range of 298–878 K in a flow reactor employing laser photolysis. From their measure ments, at 298 K, they deduced a reaction rate coefficient for the reaction $S + O_2 \rightarrow SO + O$, with $k(298\ \text{K}) = 1.15 \times 10^{12}$ cm^3 mol^{-1} s^{-1}.

They also report rate coefficients for the temperature range of 505–878 K, combining their results with data reported at high temperatures, and give a rate coefficient for $298 < T < 3460$ K, which increases slightly with the temperature

$$S + O_2 \rightarrow SO + O \qquad 5.43 \times 10^{5} \quad 2.11 \quad -730.0 \qquad (3)$$

and gives $k(1600\ \text{K}) = 4.94 \times 10^{12}$ cm^3 mol^{-1} s^{-1}. They also perform quantum chemistry calculations with Rice–Ramsperg er–Kassel–Marcus (RRKM) multichannel simulations to confirm the experimentally determined rate coefficient.

Glarborg et al.[3] referring to data collections from the literature[13] and the experiments in ref 10 derived and used the following rate coefficients in an experimental and theoretical study on the effect of SO, on moist CO oxidation with and without NO:

$$S + O_2 \rightarrow SO + O \qquad 2.0 \times 10^{6} \quad 1.93 \quad -704.6 \qquad (4)$$

with $k(1600\ \text{K}) = 1.97 \times 10^{12}$ cm^3 mol^{-1} s^{-1}. In ref 4, quoting the refs 11 and 13, the kinetic parameters for this reaction are given as

$$S + O_2 \rightarrow SO + O \qquad 5.20 \times 10^{6} \quad 1.8 \quad -600.0 \qquad (5)$$

resulting, at a combustion temperature of $T = 1600$ K, in $k = 4.43 \times 10^{12}$ cm^3 mol^{-1} s^{-1}.

With the objective of developing a kinetic scheme, Savel'ev et al.[14] in a computational study analyzed the formation kinetics of SO_x and HSO_y compounds using an extended kinetic model. They report an only slightly temperature dependent reaction rate coefficient

$$S + O_2 \rightarrow SO + O \qquad 6.32 \times 10^{11} \quad 0.5 \quad 0.0 \qquad (6)$$

giving $k(1600\ \text{K}) = 2.53 \times 10^{13}$ cm^3 mol^{-1} s^{-1}. Additionally, in ref 14, reaction rate coefficients for the subsequent oxidation reactions are given, which all exhibit non Arrhenius behavior with a decrease of the reaction rate with an increasing temperature.

$$SO + O_2 \rightarrow SO_2 + O \qquad 4.46 \times 10^{11} \quad 0.0 \quad -3268.0 \qquad (7)$$

$$SO_2 + O + M \rightarrow SO_3 + M$$

$$k_{\longrightarrow} \qquad 4.40 \times 10^{14} \quad 0.0 \quad -3196.0$$

$$k_{\longleftarrow} \qquad 3.16 \times 10^{15} \quad 0.0 \quad -32201.0 \qquad (8)$$

$$SO_3 + O \rightarrow SO_2 + O_2 \qquad 6.50 \times 10^{14} \quad 0.0 \quad -5456.0 \qquad (9)$$

Essentially, the above reported rate coefficients for the reaction $S + O_2 \rightarrow SO + O$ have their origin in the experiments of refs 10 and 11 and, lying in the order of magnitude of 10^{12}, do not differ significantly at 1600 K. They exhibit, however, different temperature dependency. Only the rate coefficients from ref 14 result in a higher value, viz., $k(1600\ \text{K}) \sim 2.5 \times 10^{13}$. These rate coefficients, which have been developed under particular experimental conditions and modeling targets, may be out of the original objectives and, consequently, may be used off topic in the framework of pure sulfur/air combustion, and it can be expected that the set of reactions selected lead to wide variations in the results. Therefore and as a result of some differences in the reported data, a revisiting of the rate coefficient of this reaction seems appropriate.

In addition to the above discussed reaction, the formation of different S/O species is important for the combustion of sulfur in a hydrogen and carbon free environment. One example is S_2O_2, and several isomers are existing for S_2O_2.[15,16] However, reaction mechanisms describing the formation of this species are not available in the literature. Frandsen et al.[17] have reported the formation of S_2O_2 in *cis* OSSO and *trans* OSSO structures formed from the addition of two SO. The experimental and numerical study of the high temperature

reaction of S + SO_2 investigated by Murakami et al.[18] has shown the formation of S_2O_2 intermediates. They have reported several structures for this S_2O_2 species, such as SSO_2, OSSO, or SOS═O. Goodarzi et al.[19] have carried out theoretical studies on the triplet and singlet potential energy surfaces for the reactions $^3S + {}^1SO_2$ and $^1S + {}^1SO_2$, respectively, and provide further information about gas phase reactions of S + SO_2.

In the present study, the rate parameters for the reaction S + O_2 → SO + O are revisited with the help of numerical simulations of premixed laminar one dimensional S_2/air flames over a wide range of equivalence ratios and quantum chemistry computations. As a result of the scarcely available kinetic data, other S/O compounds of these species as well as new developed reactions will be considered in future work. For the simulations, a starting mechanism based on the detailed reaction mechanism in ref 20, removing all reactions involving hydrogen containing species, is used resulting in 11 reactions between 9 sulfur/oxygen species. Sensitivity analysis of the computed results is performed to identify the reactions, in which rate coefficients generate the highest sensitivities with respect to the burning velocities and flame structures. Different rate parameters from the literature for this reaction are used in comparison to new quantum chemistry based rate parameters for the reaction S + O_2 ⇄ SO + O. With the help of the numerical simulations of the combustion of S_2 with air, the impact of the different rate coefficients on laminar burning velocities and species evolution were analyzed and compared. The effects of the temperature and pressure are investigated as well.

2. RESULTS AND DISCUSSION

2.1. Basic Mechanism. The reaction mechanism used in the present study is based on a detailed combustion mechanism developed by the research group of Leeds University.[20] This reaction mechanism contains initially 450 reactions and 78 species. For this study, only reactions involving species containing sulfur and oxygen are included. The resulting mechanism encompasses 11 reactions between 9 sulfur/oxygen species. The reactions and corresponding rate coefficients are listed in Table 1.

Throughout the study, the mechanism listed in Table 1 is referred to as the "basic mechanism". To find the crucial steps for the combustion of S_2, the kinetic parameters of reaction 1, which turns out to be the reaction which rate coefficients that create the highest sensitivity of the burning velocities (see section 2.2.1), are replaced by those reported in the literature. Reaction 1 is also re evaluated using the methods defined in section 3, and the rate parameters are compared to kinetic data from the literature as well. The different reaction rate coefficients for reaction 1 used in this study are listed in Table 3 along with the corresponding references.

2.2. Laminar Burning Velocities with the Basic Mechanism. One of our objectives in the collaborative research project is designing a sulfur combustor. For this, combustion characteristics of sulfur, such as flame structure and laminar burning velocities, are prerequisites. Sulfur is supplied to the burner as liquid and, similar to oil in industrial burners, is evaporated in the burner and, subsequently, to feed as vapor in the flame. Although the "fuel" is liquid at typical feed conditions, flame calculations that are used to compute combustion characteristics usually start at the gas phase,

Table 1. Basic Mechanism Used in This Study for the Oxidation of S_2 with Air Extracted from Ref 20[a]

		$k = AT^b \exp(-T_A/T)$		
	reaction	A	b	T_A
1	S + O_2 → SO + O	5.20×10^6	1.8	600.0
2	S_2 + M → 2S + M	4.80×10^{13}	0.0	38800.0
	N_2 enhanced by 1.500×10^0			
	SO_2 enhanced by 1.000×10^1			
	low pressure limit: 0.120×10^{22}, 0.154×10^1, and 0.00×10^0			
	TROE centering: 0.550×10^0, 0.100×10^{-29}, and 0.10×10^{31}			
3	S_2 + O → SO + S	1.00×10^{13}	0.0	0.0
4	SO_3 + O → SO_2 + O_2	2.00×10^{12}	0.0	10000.0
5	SO_3 + SO → $2SO_2$	1.00×10^{12}	0.0	5000.0
6	SO + O (+M) → SO_2 (+M)	3.20×10^{13}	0.0	0.0
	N_2 enhanced by 1.500×10^0			
	SO_2 enhanced by 1.000×10^1			
	low pressure limit: 0.120×10^{22}, 0.154×10^1, and 0.00×10^0			
	TROE centering: 0.550×10^0, 0.100×10^{-29}, and 0.10×10^{31}			
7	SO_2 + O (+M) → SO_3 (+M)	9.20×10^{10}	0.0	1200.0
	low pressure limit: 0.240×10^{29}, 0.400×10^1, and 0.264×10^4			
8	SO + M → S + O + M	4.00×10^{14}	0.0	54000.0
	N_2 enhanced by 1.500×10^0			
	SO_2 enhanced by 1.000×10^1			
9	SO + O_2 → SO_2 + O	7.60×10^3	2.4	1500.0
10	2SO → SO_2 + S	2.00×10^{12}	0.0	2000.0
11	SO_3 + S → SO + SO_2	5.12×10^{11}	0.0	0.0

[a] A, mol cm s K; T_A, K.

because the heat for the evaporation step in technical systems is fed back from the combustion process (flame) itself.

Using the PREMIX program from the CHEMKIN pack age,[21] the mass and energy balances for homogeneously premixed, flat, one dimensional S_2/air flames have been solved. Isobaric conditions are presumed for the calculations of flame and reaction zone structures and the corresponding laminar burning velocities. The simulations were performed for a wide range of air/S_2 ratios, and selected results are discussed for rich (λ < 1.0), stoichiometric (λ = 1.0), and lean (λ > 1.0) conditions. The results from numerical simulations are given in terms of the air/fuel ratio λ of S_2 combustion, which is defined in eq 10, with m_i being the masses of fuel and air.

$$\lambda = \frac{m_{air}/m_{fuel}}{(m_{air}/m_{fuel})\text{stoich}} \tag{10}$$

The stoichiometry is determined considering the reaction

$$S_2 + 2O_2 \rightarrow 2SO_2 \tag{11}$$

Additionally, the effect of the temperature and pressure has been evaluated. Throughout the simulations presented in section 2.2, the basic mechanism (Table 1) has been used.

In Figure 1, laminar burning velocities are plotted for two temperatures and pressures in dependence upon the air/fuel ratio λ. The left panel of Figure 1 illustrates calculations of the burning velocity at normal pressure (P = 1 atm) for two temperatures of the incoming mixture T_0 = 373 and 423 K. On the right panel of Figure 1, the effect of the pressure on S_L at T_0 = 373 K is demonstrated. The air/fuel ratio has been varied in the range of 0.2 < λ < 3.0. The results also are summarized in Table 2 for a quantitative comparison.

The calculations clearly show that the highest burning velocities for the combustion of S_2 are obtained, analogously to hydrocarbon flames, under slightly rich conditions. In the fuel rich region, 0.2 < λ < 1.0, the burning velocity as expected

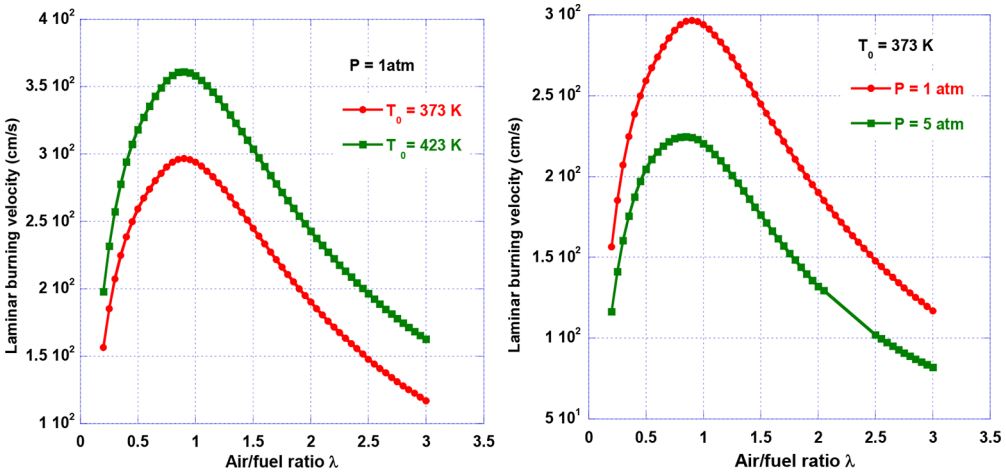

Figure 1. Laminar burning velocity for S_2/air calculated at (left) two temperatures, T_0 = 373 and 423 K, and (right) two pressures, P = 1 and 5 atm.

Table 2. Calculated Burning Velocities (cm s^{-1}) of S_2/Air at Different Air/Fuel Ratios

	fuel-rich mixture				stoichiometric	fuel-lean mixture		
basic mechanism	λ = 0.2	λ = 0.4	λ = 0.8	maximum value	λ = 1	λ = 1.5	λ = 2.0	λ = 2.5
T_0 = 423 K	197.9	294.1	358.4	λ = 0.9	358.1	303.8	242.8	196.5
P = 1 atm				361.20				
T_0 = 373 K	156.5	238.6	294.0	λ = 0.85	293.9	244.8	190.2	147.8
P = 1 atm				296.0				
T_0 = 373 K	116.4	187.4	224.4	λ = 0.85	220.4	176.3	132.0	102.2
P = 5 atm				224.70				

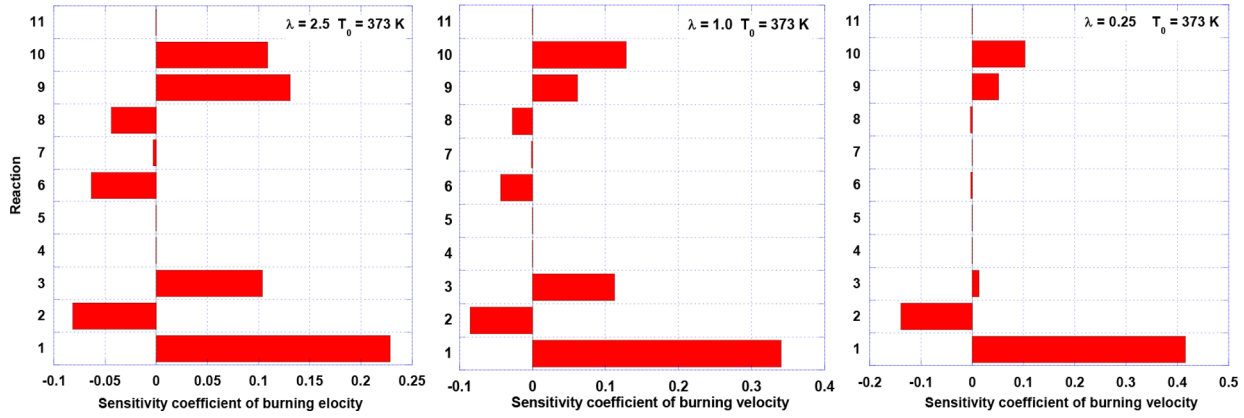

Figure 2. Sensitivity coefficients of the burning velocity with respect to the rate coefficients from Table 1 for fuel lean (λ = 2.5, left), stoichiometric ((λ = 1.0, middle), and fuel rich (λ = 0.25, right) conditions at T_0 = 373 K and P = 1 atm.

increases to attain a maximum of 296.0 cm s^{-1} at λ = 0.85 and T_0 = 373 K. Toward the fuel lean region, the burning velocity decreases. The burning velocity increases significantly at a higher temperature (T_0 = 423 K), with a maximum of 361.2 cm s^{-1} at λ = 0.90. The results exhibit unusual high burning velocities, which are unfortunately difficult to confirm because no experimental data are available. Burning velocities for the combustion of H_2S with air are comparably much smaller, although hydrogen is contained in the fuel. In ref 22, values of about 42 cm s^{-1} at stoichiometric conditions for H_2S/air are reported, and similar values and a comparison to experimental data are given in ref 23.

The laminar burning velocity was also calculated at an elevated pressure (P = 5 atm); see the right panel of Figure 1. The results show the expected decrease of the laminar burning velocities with the pressure that has been observed for combustion of numerous different fuels; see, e.g., refs 24−26. The burning velocity of S_2/air at 5 atm shows the same trend as at 1 atm and reaches a maximum of 224.7 cm s^{-1} again at λ = 0.85, which is a reduction by about 25% compared to 1 atm.

2.2.1. Sensitivity Analysis of Laminar Burning Velocities Computed with the Basic Mechanism. To identify the reaction having the most important impact on the burning velocity in the sulfur system, sensitivity analysis was performed at three air/fuel ratios, λ = 2.5 (lean), λ = 1.0 (stoichiometric), and λ = 0.25 (rich). The sensitivity coefficients K_S are defined here as the derivative of the burning velocity S_L with respect to the rate constant of reaction r, k_r, normalized by the corresponding values under unchanged conditions S_{L0} and k_{r0}.

$$K_S = \frac{dS_L}{dk_r}\frac{k_{r0}}{S_{L0}} \tag{12}$$

Table 3. Rate Coefficients for Reaction 1 from the Literature for the Flame Calculations[a]

reaction	$k = AT^b \exp(-T_A/T)$		
	A	b	T_A
$S + O_2 \rightarrow SO + O$ basic mechanism[20]	5.20×10^6	1.8	600.0
$S + O_2 \rightarrow SO + O$ Savel'ev[14]	6.32×10^{11}	0.5	0.0
$S + O_2 \rightarrow SO + O$ Glarborg[6]	5.40×10^5	2.11	729.7

[a] A, mol cm^3 s K; T_A, K.

Table 4. Calculated Laminar Burning Velocities (cm s^{-1}) of S_2/Air with Different Rate Coefficients for Reaction 1, with T_0 = 373 K and P = 1 atm

	rich mixture				stoichiometric	lean mixture		
mechanism	λ = 0.2	λ = 0.4	λ = 0.8	maximum value	λ = 1	λ = 1.5	λ = 2.0	λ = 2.5
basic mechanism[20]	156.5	238.6	294.0	λ = 0.85 296.0	293.9	244.8	190.2	147.8
Savel'ev[14]	371.1	507.7	541.6	λ = 0.7 548.5	506.0	388.6	300.4	238.3
Glarborg[6]	152.8	234.2	289.5	λ = 0.90 292.2	289.7	240.9	186.2	144.4

The sensitivity coefficients reflect a relative change of the model response, caused by a relative change of the rate coefficient of a specific reaction.

As seen in Figure 2, the highest sensitivity coefficients of the burning velocity at 1 atm and T_0 = 373 K result for the rate coefficient of reaction 1, $S + O_2 \rightarrow SO + O$, exhibiting an increase with decreasing λ. For fuel rich flames, e.g., a ±10% change in the rate coefficient of this reaction would increase the burning velocity by approximately ±5%. The sensitivity coefficients of all other rate coefficients are similar in the fuel lean and stoichiometric regions, and the corresponding reaction rates show a significant lower impact on S_L. Under fuel rich conditions, the impact of reaction 1 on the burning velocity is not only as important as for the other mixture compositions but is nearly the only determinant reaction. A much smaller impact is exerted by reaction 2, $S_2 + M \rightarrow 2S + M$, followed by the disproportionation of SO to SO_2 and S, reaction 10, in an even lower level of magnitude.

2.3. Discussion of Rate Coefficients for Reaction $S + O_2 \rightarrow SO + O$ from the Literature. On the basis of the findings of the sensitivity analysis revealing that the rate coefficient of reaction 1 creates the highest sensitivity coefficient of the burning velocity of S_2 with air, different rate coefficients reported in the literature and listed in Table 3 have been included in the numerical simulations of laminar premixed one dimensional flames.

2.3.1. Burning Velocities with Rate Coefficients of Reaction $S + O_2 \rightarrow SO + O$ from the Literature. The burning velocities obtained at T_0 = 373 K and P = 1 atm with the basic mechanism as reported above are compared to those obtained with the reaction mechanisms of Savel'ev[14] and Glarborg.[6] The differences in the reaction mechanism are the rate coefficients of reaction 1. The computed laminar burning velocities (see Table 4 and Figure 3) show all over the same behavior as those estimated with the basic mechanism. It appears that the burning velocity calculated with the rate coefficient from ref 14 is by far faster than all other burning velocities. This could be understood with the comparative high value of the rate coefficient and from the high sensitivity of the burning velocity with respect to this rate coefficient. The maximum burning velocity is obtained in the fuel rich region with 548.5 cm s^{-1} at λ = 0.7. The rate coefficient from the basic mechanism[20] results in a somewhat slower burning velocity of 296.0 cm s^{-1} at λ = 0.85, revealing again the importance of this rate coefficient. The rate coefficient for reaction 1 in ref 4 appears to be the smallest rate coefficient and, consequently, produces the lowest burning velocity with 292.2 cm s^{-1} at λ = 0.90.

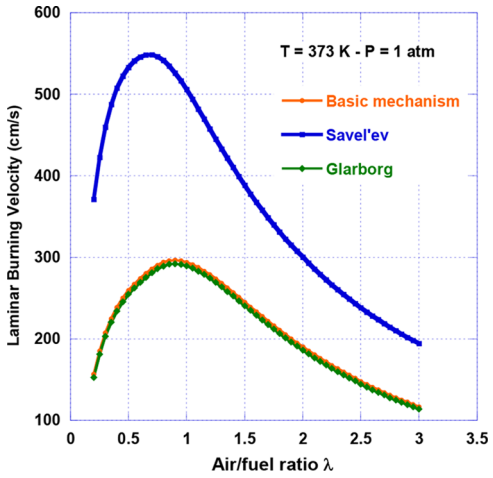

Figure 3. Laminar burning velocity for S_2/air λ calculated with the rate coefficients for reaction 1 from Table 3, with T_0 = 373 K and P = 1 atm.

In summary, the computed burning velocities employing the rate coefficients given in Table 3 apparently produce unusual high burning velocities. Therefore, the rate coefficient of reaction 1 is examined in more detail.

3. CALCULATION OF THE REACTION RATE COEFFICIENT OF $S + O_2 \leftrightarrow SO + O$ WITH QUANTUM CHEMISTRY METHODS

With the help of quantum chemistry methods, the kinetic parameters for the reaction $S + O_2 \rightarrow SO + O$ have been revisited and the resulting laminar burning velocity and species concentration profiles for one dimensional laminar premixed S_2/air flames have been examined.

3.1. Applied Methods. The thermochemical properties of all species involved in reaction 1 have been calculated with the help of several computational methods using the Gaussian 09 program

suite.[27,28] Previous results[29] have shown that all density functional theory (DFT) calculations give poor outcome in estimating the enthalpies of reactions involving S_2. Therefore, six composite methods (*ab initio*) were tested (G2,[30] G3,[31] G3MP2,[32] G3MP2B3,[33] G3B3,[34] and CBS QB3[35]). Finally, because of its reliability, the enthalpies resulting from the well regarded CBS QB3 are selected for use in the present sulfur/air system.

The reaction rate coefficients of reaction 1 were estimated using the canonical transition state theory (TST).[36] The ThermKin code[37] was used to determine the elementary reaction rate coefficients and to express the rate coefficients in the modified Arrhenius form (see Tables 1 and 3). ThermKin also converts thermochemical properties to the National Aeronautics and Space Administration (NASA) polynomial format required for simulations with CHEMKIN. From the kinetic analysis, high pressure rate coefficients for each channel are obtained from the calculated energies, vibration frequencies, and structures. The modified Arrhenius parameters are determined from regression analysis with application of the principle of least squares.

Thermodynamic and transport data of all species required for the numerical simulations with CHEMKIN and not specifically mentioned as well as the rate coefficients have been taken from the Supporting Information of ref 7.

3.2. Estimation of the S + O_2 → SO + O Reaction as an Abstraction Reaction. The burning velocity calculations above show that the simulations with the rate parameters for the overall S + O_2 → SO + O reaction, which are only a little dependent upon temperature (see Table 3), yield comparatively high burning velocities. One approach for refinement of these rate coefficients is to consider the S atom abstracting one oxygen atom from O_2 and forming SO + O. Figure 4 shows a perfect displacement of middle

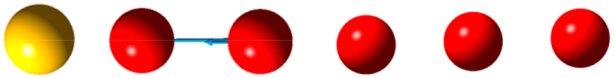

Figure 4. Transition state structures of (left) S−O−O and (right) O−O−O.

oxygen between S and O with an imaginary frequency of −1234.6 cm^{-1} on a triplet surface. It has also been identified on a singlet and quintuplet surface. In this linear transition state structure, the S−O bond length is at 1.8398 Å and the O−O bond length is at 1.5233 Å. In an analogy, O_3 (to O_2 + O) has shown the same kind of transition state, with the O−O—O bond lengths at 1.5098 and 1.510 03 Å. For this O_3 dissociation to O_2 + O, the same type of transition state structure (imaginary frequency = −1038.5 cm^{-1}) has been observed, as illustrated on the right of Figure 4.

The calculation of enthalpy for the S−O−O abstraction transition state structure has resulted in a high barrier near 60 kcal mol^{-1}. Ref 12 reports a similar value (54.4 kcal mol^{-1}) on a quintuplet surface. This is clearly not in agreement with the approximate barrier less reaction reported in the literature. While this is an interesting transition state structure, it does not explain the reaction process and is further not considered.

A second approach is to consider the association of S + O_2 to form an energized SOO* adduct, which can further react to SO + O or dissociate back to S + O_2

$$S + O_2 \rightleftarrows SOO^* \rightarrow SO + O \quad (13)$$

and

$$SOO^* \rightleftarrows SOO \quad (14)$$

The addition of O_2 to S occurs without a barrier to form SOO calculated at the CBS QB3 calculation level.[35] This structure is illustrated in the potential diagram in Figure 6. This association reaction can occur on two different potential surfaces: a singlet surface, where the non paired electrons of the S atom and the O atom are of opposite spins, or a triplet surface.[12] Studies performed on oxygenated hydrocarbons have shown that the addition of O_2 is without a barrier[38] or with some 0.9 kcal mol^{-1} only.[39] The formation of this SOO intermediate has also been reported in the work of Lu et al.[12] They have calculated different geometries for SOO, which then reacts further to SO + O or leads to SO_2 formation, depending upon the multiplicity (0 or 3) and the temperature.

In this work, also two geometries as illustrated in Figure 5 were identified. For this angular SOO, the geometry on the left of Figure 5

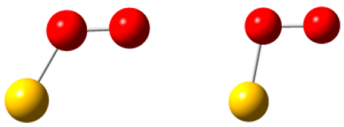

Figure 5. Geometry of the (left) SOO singlet and (right) SOO triplet.

corresponds to the singlet state and the geometry on the right of Figure 5 corresponds to the triplet state. The dissociation of the singlet and triplet structures leads to SO + O. We note that the system can also react to SO_2. This last reaction is not investigated in this study. The geometries are in good agreement with those reported by Lu et al.[12]

For the present, we consider that the formation and dissociation of the SOO intermediate to SO + O and back to S + O_2 are determining the overall kinetics of the reaction

$$S + O_2 \rightleftarrows SOO^* \rightarrow SO + O \quad (15)$$

The formation of SOO from both the triplet and singlet reactant sets was included. The barrier needed for the dissociation of SOO is derived from the O−O distance. Using the structure illustrated in Figure 6, the new parameters are calculated as follows: first, the

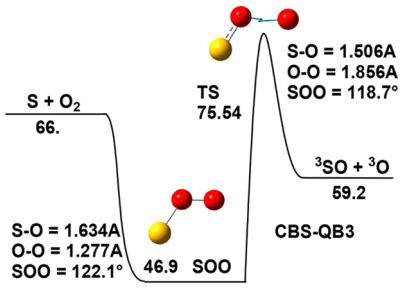

Figure 6. Potential diagram of S + O_2 ↔ SOO* ↔ SO + O (kcal mol^{-1}). ↓ and ↑ SOO°

formation of SOO from S + O_2 association and then the dissociation of SOO to SO + O. To determine the barrier needed for the dissociation of SOO, the O−O distance at which the terminal oxygen moves away from the second oxygen is taken. This O−O distance corresponds to 1.856 Å (see TS in Figure 6) and to an imaginary frequency of −288.9 cm^{-1}. This structure also shows the SO double bond being formed. We point out that, in their paper, Lu et al. have identified several transition states for this reaction and defined that the lowest barrier corresponds to the transition state structure at O−O = 1.705 Å.[12] Using the structure illustrated in Figure 6 we have calculated reaction rate parameters as given in Table 5.

The newly calculated rate parameters exhibit a much stronger dependency upon the temperature than those from the literature (see Tables 3 and 5), leading to values at 1600 K, which are about 1 order of magnitude lower. Using parameters of Table 5, the burning velocities have been recalculated.

3.3. Laminar Burning Velocity with Calculated Reaction Rate Parameters of Reaction 1. Using the rate parameters from Table 5, the laminar burning velocities have been calculated in dependence upon the air/fuel ratio for two temperatures, T_0 = 373 and 423 K, and two pressures, P = 1 and 5 atm. Figure 7 illustrates the results for atmospheric pressure for two temperatures, T_0 = 373 and 423 K (left), and the effect of the pressure at T_0 = 373 K (right). The

Table 5. Calculated Rate Parameters for the Formation of SO[a]

overall reaction rate from master equation analysis		$k = AT^b \exp(-T_A/T)$ A	b	T_A
$S + O_2 \rightarrow SO + O$	singlet	2.69×10^{10}	0.15	5358.8
$k(1600\ K) = 2.86 \times 10^9$				
$S + O_2 \rightarrow SO + O$	triplet	1.09×10^{11}	0.15	2369.4
$k(1600\ K) = 7.50 \times 10^{10}$				

[a] A, mol cm^3 s K.

S_2/air ratio has been varied in the range of $0.2 < \lambda < 3.0$. The results demonstrate that, apparently, the utilization of the refined rate parameters slows the burning velocity considerably. The highest value is 92.6 cm s^{-1}, obtained at T = 423 K and λ = 1.1, which is somewhat in the lean region (compare to Table 6). The calculated laminar burning velocity is in the order of magnitude of the burning velocity of H_2S/air mixtures.[22,23]

At elevated pressure of P = 5 atm (right panel of Figure 7), S_L decreases with pressure. The burning velocity of the S_2/air flame at P = 5 atm attains a maximum of 65.4 cm s^{-1} at λ = 1.05. We note that these results should be considered preliminary, and we look for experimental values of the flame speed to improve the reaction mechanism.

3.4. Sensitivity Analysis of Laminar Burning Velocities for Calculated Rate Parameters. As in section 2.2.1, a sensitivity analysis of the laminar burning velocity with respect to the rate coefficients of the refined mechanism has been performed for three equivalence ratios, λ = 2.5 (lean), λ = 1.0 (stoichiometric), and λ = 0.25 (rich) conditions. The results for stoichiometric and fuel rich conditions are plotted in Figure 8.

Figure 8 reveals that, whatever the level of the fuel/air ratio, reaction 1 no longer has impact on the burning velocity. The explanation lies in the significantly stronger temperature dependency compared to the rate coefficient in the basic mechanism. Figure 8 also demonstrates that, with the modified rate coefficient for reaction 1, the burning velocity exhibits by far the highest sensitivity with respect to the reaction rate coefficient of the oxidation of SO to SO_2, reaction 9, $SO + O_2 \rightarrow SO_2 + O$, at stoichiometric and fuel rich conditions. The results from fuel lean conditions, not shown in the Figure 8, confirm these trends.

3.5. Species Mole Fraction and Temperature Profiles. Figures 9 and 10 represent mole fraction profiles for the most important reaction partners in the combustion of S_2 with air from the CHEMKIN simulations. Figure 9 reveals that, under fuel lean (λ = 2.5, left) and stoichiometric (λ = 1, middle) conditions, S_2 is converted completely and rapidly into SO_2 with some excess of oxygen. Comparably, under fuel lean conditions (λ = 0.25, right), oxygen is completely consumed. In parallel, for all mixture fractions, SO_2 formation increases steadily to attain a maximum at stoichiometric conditions. At fuel rich conditions (right), the S_2 mole fraction decreases until no oxygen is available and then starts to increase again. The amount of reformed S_2 is approximately 21%.

In Figure 10, the mole fraction profiles for SO, S, SO_3, and O are represented for three air/fuel ratios, λ = 2.5, 1.0, and 0.25. As seen, the maximum concentration of SO and S are calculated at stoichiometric conditions, while at fuel lean conditions, little SO and S is formed. Under fuel rich conditions, SO and S are also important but their consumption is slow.

The formation of SO_3 is at its maximum at fuel lean conditions. At stoichiometric conditions, SO_3 formation is markedly lower and SO_3 is rapidly consumed. With the lack of oxygen, the mole fraction of SO_3 is negligible.

The left panel of Figure 11 illustrates the temperature profiles for three S_2/air equivalence ratios, and the right panel of Figure 11 illustrates the corresponding flow velocity profiles in the one dimensional reaction zone. As seen in the left panel of Figure 11, for the three air/fuel ratios, the temperature (with $T_{initial}$ = 373 K) increases steeply in the reaction zone and approaches a temperature plateau. As expected, the final temperature at lean conditions (λ = 2.5) is the lowest at about 1350 K. At fuel rich conditions, λ = 0.25, the flame temperature reaches 1600 K and is above 2000 K at stoichiometric conditions, which is comparably as high as in hydrocarbon/air flames.[40] It is important to point out that, at stoichiometric conditions, the temperature reaches its maximum value, as shown in Figure 11, and, therefore, considerably accelerates the further reaction of the primary products.

Additionally, in the right panel of Figure 11, the profiles of the flow velocity in the one dimensional reaction zone are plotted. The steep increase of the flow velocity can be associated with the acceleration as a result of the thermal expansion caused by the heat release of the flame. The flow velocity at inlet conditions represents the burning velocity. Using the calculated rate coefficients for reaction 1 (Table 5), the laminar burning velocity is in the order of magnitude comparable to the burning velocity of hydrocarbons. Using rate coefficients from the literature for the calculation of the laminar burning velocity results in nearly 10 times faster burning velocities

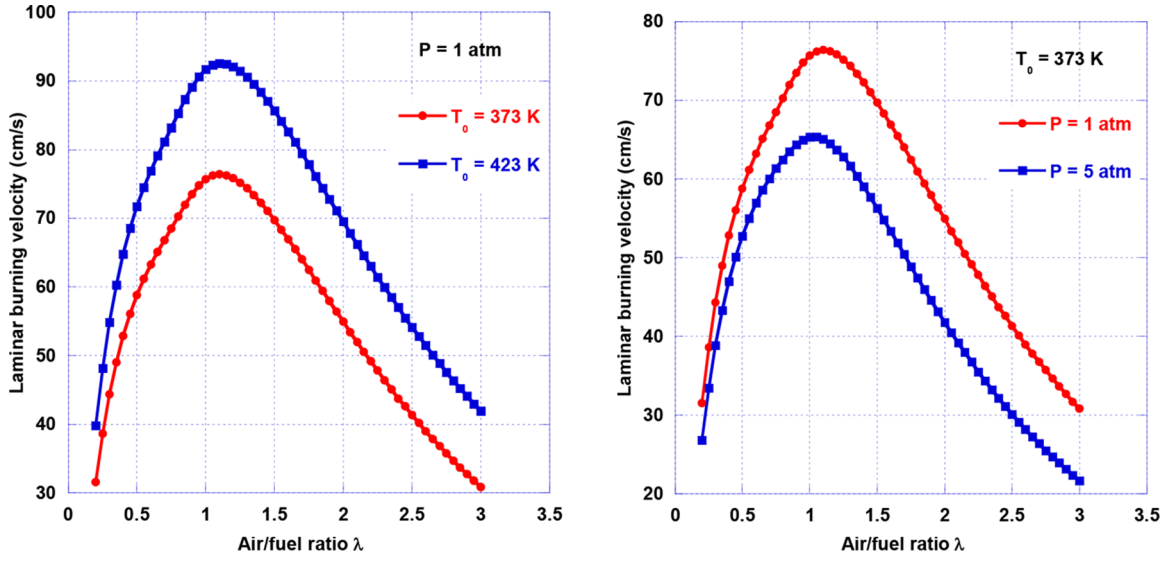

Figure 7. Laminar burning velocity with revised rate coefficients for S_2/air calculated at T_0 = 373 and 423 K and P = 1 and 5 atm.

Table 6. Calculated Flame Velocities (cm s^{-1}) of S_2/Air with Refined Kinetic Parameters for Reaction S + O_2 → SO + O, with T_0 = 373 K and P = 1 atm

	rich mixture				stoichiometric	lean mixture		
refined k_1	λ = 0.2	λ = 0.4	λ = 0.8	maximum value	λ = 1	λ = 1.5	λ = 2.0	λ = 2.5
T = 423 K	39.79	64.77	85.30	λ = 1.1	91.70	85.68	69.51	54.13
P = 1 atm				92.59				
T_0 = 373 K	31.57	52.85	70.27	λ = 1.1	75.70	69.71	54.94	41.32
P = 1 atm				76.41				
T = 373 K	26.85	47.01	62.48	λ = 1.05	65.33	56.30	41.80	30.11
P = 5 atm				65.37				

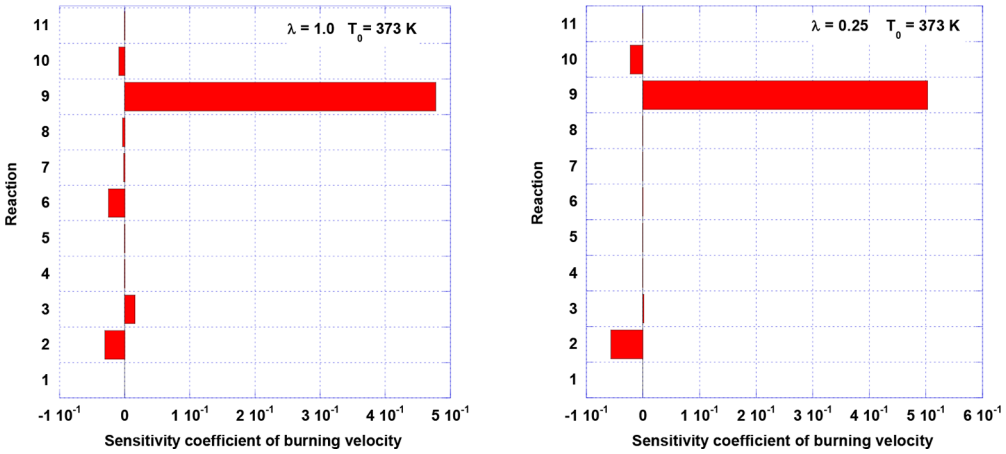

Figure 8. Sensitivity coefficients of the burning velocity with respect to the rate coefficients of the refined mechanism at stoichiometric and rich conditions (λ = 1 and 0.25).

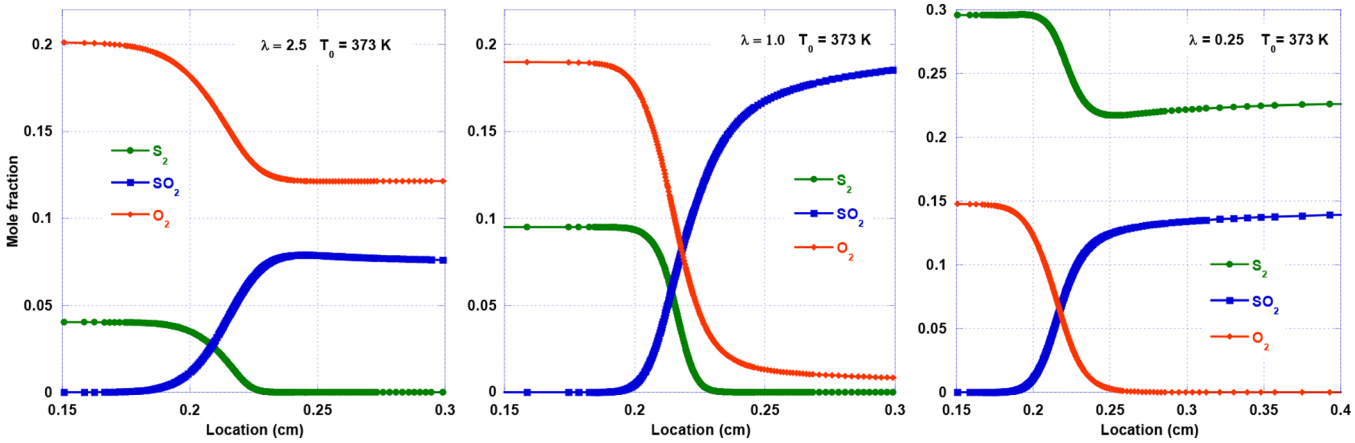

Figure 9. Mole fraction profiles of the major species for S_2/air flames for (left) λ = 2.5, (middle) λ = 1.0, and (right) λ = 0.25.

than typical burning velocities for hydrocarbon/air flames and more comparable to hydrogen flames.[41,42]

4. CONCLUSION

The oxidation of S_2 for a wide range of air/fuel ratios has been investigated with the help of numerical flame calculations. In a first approach, a reaction mechanism was employed that has been derived from a detailed H/O/S combustion mechanism, removing all reactions involving hydrogen species. Flame calculations with this mechanism exhibited unusual high laminar burning velocities.

For that reason, sensitivity analysis of the burning velocity with respect to the rate parameters of all reactions was performed, indicating that the highest sensitivity coefficients of the laminar burning velocity are created by the reaction rate coefficient of the reaction S + O_2 → SO + O. For this reaction, new reaction rate parameters were calculated with the help of quantum chemistry methods. The new reaction rate parameters indicate a stronger temperature dependency compared to the corresponding rate coefficients from the literature.

Laminar burning velocities based on that reaction rate parameter are lower by about a factor of $^1/_{10}$, strongly dependent upon the temperature and pressure, and comparable to the burning velocities of, e.g., H_2S with air. Sensitivity analysis brings about the fact that these changes modify the sensitivity of the burning velocity for the conversion of S_2 to different reactions, e.g., the reaction of SO + O_2 → SO_2 + O. The reaction rate parameters of these

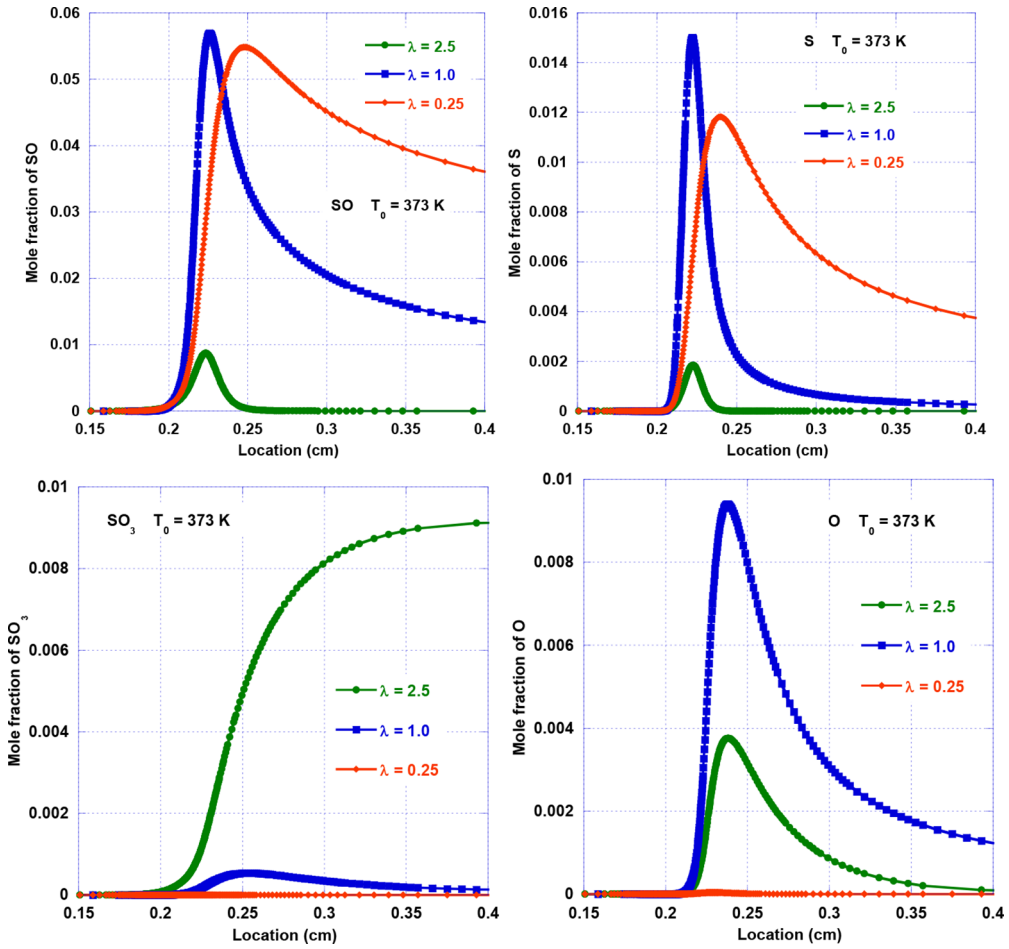

Figure 10. Mole fraction profiles of minor species for S_2/air flames at λ = 2.5, 1.0, and 0.25.

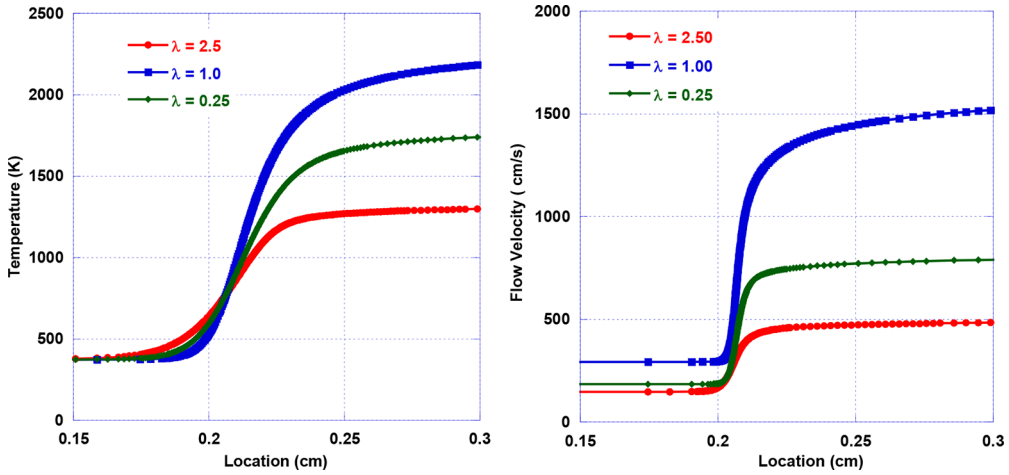

Figure 11. Calculated temperature profiles and flow velocities for three S_2/air flames with (lean) λ = 2.5, (stoichiometric) λ = 1.0, and (rich) λ = 0.25 at T = 373 K and P = 1 atm.

reactions have to be evaluated also in future work for the combustion of sulfur.

AUTHOR INFORMATION

Corresponding Author

*E mail: nadia.sebbar@kit.edu.

P. Habisreuther: 0000 0003 4979 4334

J. W. Bozzelli: 0000 0003 4822 150X

Notes

The authors declare no competing financial interest.

ACKNOWLEDGMENTS

The results presented in this study have been obtained within the framework of the PEGASUS Project. This project has

received funding from the European Union's Horizon 2020 Research and Innovation Program under Grant Agreement 727540.

REFERENCES

(1) European Commission (EC). *PEGASUS (H2020 LCE 2016 2017): Renewable Power Generation by Solar Particle Receiver Driven Sulphur Storage Cycle. Horizon 2020. Competitive Low Carbon Energy*; EC: Brussels, Belgium, 2016.
(2) Louie, D. K. *Handbook of Sulphuric Acid Manufacturing*; DKL Engineering: Toronto, Ontario, Canada, 2005.
(3) Glarborg, P.; Kubel, D.; Dam Johansen, K.; Chiang, H. M.; Bozzelli, J. W. *Int. J. Chem. Kinet.* **1996**, *28*, 773−790.
(4) Alzueta, M. U.; Bilbao, R.; Glarborg, P. *Combust. Flame* **2001**, *127*, 2234−2251.
(5) Giménez López, J.; Martínez, M.; Millera, A.; Bilbao, R.; Alzueta, M. U. *Combust. Flame* **2011**, *158*, 48−56.
(6) Glarborg, P.; Marshall, P. *Int. J. Chem. Kinet.* **2013**, *45*, 429−439.
(7) Song, Y.; Hashemi, H.; Christensen, J. M.; Zou, C.; Haynes, B. S.; Marshall, P.; Glarborg, P. *Int. J. Chem. Kinet.* **2017**, *49*, 37−52.
(8) Mueller, M. A.; Yetter, R. A.; Dryer, F. L. *Int. J. Chem. Kinet.* **2000**, *32*, 317−339.
(9) Zhang, Y.; Yang, H.; Zhou, J.; Wang, Z.; Liu, J.; Cen, K. *Appl. Energy* **2014**, *130*, 396−402.
(10) Woiki, D.; Roth, P. *Int. J. Chem. Kinet.* **1995**, *27*, 59−71.
(11) Tsuchiya, K.; Kamiya, K.; Matsui, H. *Int. J. Chem. Kinet.* **1997**, *29*, 57−66.
(12) Lu, C. W.; Wu, Y. J.; Lee, Y. P.; Zhu, S.; Lin, M. C. *J. Chem. Phys.* **2004**, *121*, 8271−8278.
(13) Atkinson, R.; Baulch, D. L.; Cox, R. A.; Hampson, R. F.; Kerr, J. A.; Rossi, M. J.; Troe, J. *J. Phys. Chem. Ref. Data* **1997**, *26*, 1329−1499.
(14) Savel'ev, A. M.; Starik, A. M.; Titova, N. S. *Combust., Explos. Shock Waves* **2002**, *38* (6), 609−621.
(15) Marsden, C. J.; Smith, B. J. *Chem. Phys.* **1990**, *141*, 335−353.
(16) Ramirez Solis, A.; Jolibois, F.; Maron, L. *Chem. Phys. Lett.* **2011**, *510*, 21−26.
(17) Frandsen, B. N.; Wennberg, P. O.; Kjaergaard, H. G. *Geophys. Res. Lett.* **2016**, *43*, 11,146−11,155.
(18) Murakami, Y.; Onishi, S.; Kobayashi, T.; Fujii, N.; Isshiki, N.; Tsuchiya, K.; Tezaki, A.; Matsui, H. *J. Phys. Chem. A* **2003**, *107*, 10996−11000.
(19) Goodarzi, M.; Vahedpour, M.; Nazari, F. *Chem. Phys. Lett.* **2010**, *494*, 315−322.
(20) Hughes, K. J.; Blitz, M. A.; Pilling, M. J.; Robertson, S. H. *Proc. Combust. Inst.* **2002**, *29*, 2431−2437. and on the website of Leeds University.
(21) Kee, R. J.; Rupley, F. M.; Miller, J. A.; Coltrin, M. E.; Grcar, J. F.; Meeks, E.; Moffat, H. K.; Lutz, A. E.; Dixon Lewis, G.; Smooke, M. D.; Warnatz, J.; Evans, G. H.; Larson, R. S.; Mitchell, R. E.; Petzold, L. R.; Reynolds, W. C.; Caracotsios, M.; Stewart, W. E.; Glarborg, P.; Wang, C.; Adigun, O. *CHEMKIN Collection, Release 3.6*; Reaction Design, Inc.: San Diego, CA, 2000.
(22) Vervisch, L.; Labegorre, B. *Proceedings of the European Combustion Meeting*; Orléans, France, Oct 25−28, 2003; Paper 216.
(23) Pio, G.; Barba, D.; Palma, V.; Salzano, E. *Proceedings of the 25th International Symposium on Chemical Reaction Engineering (ISCRE25)*; Florence, Italy, May 20−23, 2018.
(24) (a) Ranzi, E.; Frassoldati, A.; Grana, R.; Cuoci, A.; Faravelli, T.; Kelley, A. P.; Law, C. K. *Prog. Energy Combust. Sci.* **2012**, *38*, 468−501. (b) Burluka, A. A.; Harker, M.; Osman, H.; Sheppard, C. G. W.; Konnov, A. A. *Fuel* **2010**, *89*, 2864−2872. (c) Chong, C. T.; Hochgreb, S. *Combust. Flame* **2011**, *158*, 490−500. (d) Gillespie, F.; Metcalfe, W. K.; Dirrenberger, P.; Herbinet, O.; Glaude, P. A.; Battin Leclerc, F.; Curran, H. J. *Energy* **2012**, *43*, 140−145.
(25) Kochar, Y.; Seitzman, J.; Lieuwen, T.; Metcalfe, W. K.; Burke, S.; Curran, H.; Krejci, M.; Lowry, W.; Petersen, E.; Bourque, G. *Proceedings of the ASME Turbo Expo 2011*; Vancouver, British Columbia, Canada, June 6−10, 2011.
(26) Sebbar, N.; Habisreuther, P.; Bockhorn, H.; Auzmendi Murua, I.; Bozzelli, J. W. *Energy Fuels* **2017**, *31*, 2260−2273.
(27) Frisch, M. J.; Trucks, G. W.; Schlegel, H. B.; Scuseria, G. E.; Robb, M. A.; Cheeseman, J. R.; Zakrzewski, V. G.; Montgomery, J. A., Jr.; Stratmann, R. E.; Burant, J. C.; Dapprich, S.; Millam, J. M.; Daniels, A. D.; Kudin, K. N.; Strain, M. C.; Farkas, O.; Tomasi, J.; Barone, V.; Cossi, M.; Cammi, R.; Mennucci, B.; Pomelli, C.; Adamo, C.; Clifford, S.; Ochterski, J.; Petersson, G. A.; Ayala, P. Y.; Cui, Q.; Morokuma, K.; Salvador, P.; Dannenberg, J. J.; Malick, D. K.; Rabuck, A. D.; Raghavachari, K.; Foresman, J. B.; Cioslowski, J.; Ortiz, J. V.; Baboul, A. G.; Stefanov, B. B.; Liu, G.; Liashenko, A.; Piskorz, P.; Komaromi, I.; Gomperts, R.; Martin, R. L.; Fox, D. J.; Keith, T.; Al Laham, M. A.; Peng, C. Y.; Nanayakkara, A.; Challacombe, M.; Gill, P. M. W.; Johnson, B.; Chen, W.; Wong, M. W.; Andres, J. L.; Gonzalez, C.; Head Gordon, M.; Replogle, E. S.; Pople, J. A. *Gaussian 03, Revision A.1*; Gaussian, Inc.: Wallingford, CT, 2003.
(28) http://www.gaussian.com/index.htm.
(29) Sebbar, N.; Bozzelli, J. W.; Bockhorn, H.; Trimis, D. *Combust. Sci. Technol.* **2018**, 1.
(30) Curtiss, L. A.; Raghavachari, K.; Trucks, G. W.; Pople, J. A. *J. Chem. Phys.* **1991**, *94* (11), 7221−7230.
(31) Curtiss, L. A.; Raghavachari, K.; Redfern, P. C.; Rassolov, V.; Pople, J. A. *J. Chem. Phys.* **1998**, *109* (18), 7764−7776.
(32) Curtiss, L. A.; Redfern, P. C.; Raghavachari, K.; Rassolov, V.; Pople, J. A. *J. Chem. Phys.* **1999**, *110* (10), 4703−4709.
(33) Baboul, A. G.; Curtiss, L. A.; Redfern, P. C.; Raghavachari, K. *J. Chem. Phys.* **1999**, *110* (16), 7650−7657.
(34) Anantharaman, B.; Melius, C. F. *J. Phys. Chem. A* **2005**, *109*, 1734−1747.
(35) Montgomery, J. A., Jr.; Frisch, M. J.; Ochterski, J. W.; Petersson, G. A. *J. Chem. Phys.* **1999**, *110* (6), 2822−2827.
(36) Steinfeld, J. I.; Francisco, J. S.; Hase, W. L. *Chemical Kinetics and Dynamics*; Prentice Hall, Inc., A Simon & Schuster Company: Englewoods, NJ, 1989; p 07632.
(37) Sheng, C. Ph.D. Dissertation, Department of Chemical Engineering, Chemistry and Environmental Science, New Jersey Institute of Technology, Newark, NJ, 2002.
(38) Tokmakov, I. V.; Kim, G. S.; Kislov, V. V.; Mebel, A. M.; Lin, M. C. *J. Phys. Chem. A* **2005**, *109*, 6114−6127.
(39) Sebbar, N.; Bozzelli, J. W.; Bockhorn, H. *J. Phys. Chem. A* **2014**, *118*, 21−37.
(40) Andrews, G. E.; Bradley, D. *Combust. Flame* **1972**, *19* (2), 275−88.
(41) Milton, B. E.; Keck, J. C. *Combust. Flame* **1984**, *58* (1), 13−22.
(42) Dahoe, A. E. *J. Loss Prev. Process Ind.* **2005**, *18* (3), 152−66.